Biosensors and Bioelectronics 77 (2016) 385–392

Contents lists available at ScienceDirect

Biosensors and Bioelectronics

journal homepage: www.elsevier.com/locate/bios

Real-time concentration monitoring in microfluidic system via plasmonic nanocrescent arrays

Bingpu Zhou [a,b], Xiao Xiao [b], Ting Liu [c], Yibo Gao [d], Yingzhou Huang [c], Weijia Wen [a,b,*]

[a] Nano Science and Technology Program and KAUST-HKUST Micro/Nanofluidic Joint Laboratory, The Hong Kong University of Science and Technology, Clear Water Bay, Kowloon, Hong Kong
[b] Department of Physics, The Hong Kong University of Science and Technology, Clear Water Bay, Kowloon, Hong Kong
[c] Soft Matter and Interdisciplinary Research Institute, College of Physics, Chongqing University, Chongqing 400044, China
[d] Environmental Science Programs, School of Science, The Hong Kong University of Science and Technology, Clear Water Bay, Kowloon, Hong Kong

ARTICLE INFO

Article history:
Received 20 July 2015
Received in revised form
3 September 2015
Accepted 23 September 2015
Available online 28 September 2015

Keywords:
Nanocrescent
Surface plasmon resonance
Microfluidics
Biosensor

ABSTRACT

In this work, on-chip bio/chemical sensor was reported based on localized surface plasmon resonance of nanocrescent patterns fabricated via electron beam lithography. The nanocrescent arrays with different dimensional features exhibited controllable plasmonic properties in accordance with the simulation results based on the finite-difference time-domain model. The highest refractive index sensitivity of the fabricated samples was achieved to be ~699.2 nm/RIU with a figure of merit of ~3.1 when the two opposite crescents own a gap of ~43.3 nm. Such obtained plasmonic sensor was further integrated into the microfluidic system which can simply control the specific analyte concentrations via tuning the flow rate ratios between two injecting microstreams. Our method has successfully demonstrated the capability of the nanocrescent patterns as on-chip plasmonic bio/chemical sensor for real-time monitoring of dynamic concentrations in the microchannel.

1. Introduction

Real-time probing of analyte concentration precisely in microfluidic systems is pivotal for characterizing various biological processes such as cell singaling, immune response, etc. (Ahmed et al., 2010; Fosser and Nuzzo, 2003; Xiao et al., 2013). As one of the most common techniques, microscopy has been proved to be efficient to produce information of on-chip bio/chemical concentrations (Mensack et al., 2013). However, the general requirement of fluorescent or chemiluminescent molecules in biological system limits its prominent application to some extent. Electrochemical sensing with integrated sensing electrodes in microfluidic channel is another well-employed approach for concentration monitoring (Gencoglu and Minerick, 2014; Yoon et al., 2014). The electrical contact between external power supply and the bioactive targets may unfortunately bring unrecoverable damages to the bio/chemical objects.

Among the numerous measuring approaches, optofluidics has been recently explored as an advanced method for on-chip bio/chemical assays (Schmidt and Hawkins, 2011). During the past decade, the combination of optics and microfluidics has served as a versatile platform for on-chip particle manipulation, imaging, or bio/chemical sensing, etc. (Erickson et al., 2011; Estevez et al., 2014; Pang et al., 2012). Localized surface plasmon resonance (LSPR) based on nano-particles or nano-patterns can significantly concentrate light into nano-scale region, which further effectively monitor the refractive index (RI) change of the medium close to the plasmonic surface (Stewart et al., 2008). To date, kinds of materials (gold, silver, etc.) and nano-patterns (prism, ring, crescent, etc.) have been well presented to be capable of sensing the RI based on the LSPR effect (Chen et al., 2008; Mannelli and Marco, 2010; Rycenga et al., 2011; Toma et al., 2014). However, rare demonstrations have been focused on adopting such plasmonic structures as integrated sensor in microfluidic system for real-time dynamic concentration monitoring (Huang et al., 2012; Escobedo et al., 2013).

Generating controllable bio/chemical concentrations in microfluidic system plays an important role in understanding complex biological aspects. One frequently used method is based on the intrinsic laminar characteristics of fluids in microscale with peripheral active or passive control (Ahmed et al., 2013; Jeon et al., 2000). In light of above, microfluidic system with capability of generating tunable concentrations as well as real-time probing is

* Corresponding author at: Nano Science and Technology Program and KAUST-HKUST Micro/Nanofluidic Joint Laboratory, The Hong Kong University of Science and Technology, Clear Water Bay, Kowloon, Hong Kong. Fax: +852 23581652.
E-mail address: phwen@ust.hk (W. Wen).

http://dx.doi.org/10.1016/j.bios.2015.09.054
0956-5663/

of great importance in the future complex on-chip bio/chemical processes. Limited research has yet concentrated on generation of dynamically controllable analyte concentrations combined with real-time on-chip effective and accurate concentration monitoring (Morel et al., 2012; Toetsch et al., 2009). In this work, we first designed and fabricated nanocrescent samples via electron beam lithography (EBL) with different geometries. Nanocrescent (NC) structure is one of the most common adopted plasmonic bio/chemical sensors due to the well-tunable LSPR property, highly confined electric field, etc. (Bukasov and Shumaker-Parry, 2007; Bukasov et al., 2010; Fischer et al., 2011). EBL was utilized to produce NC arrays with well controlled shapes and locations on the substrate which can facilitates ease of integration with the microfluidic system. The RI sensitivities were then systematically investigated and compared by using sodium chloride (NaCl) solution with different concentrations. Finally, one of the fabricated NC arrays was integrated into a microfluidic concentration gradient generator for real-time monitoring of dynamic analyte concentrations. The presented results are encouraging and convenient to be applied for on-chip monitoring of bio/chemical targets in the future.

2. Methods and materials

2.1. Design and fabrication of NC arrays

Fig. 1a illustrates the three-dimensional configuration of NC arrays patterned on a quartz substrate. It should be noted that here in the figure only paired NC arrays are depicted while in this work, both of single and paired NC were fabricated and investigated. P indicates the periodicity in both *X* (minor axis) and *Y* (major axis) directions between each individual NC unit. For the single and paired NC patterns, P is defined of 600 nm and the dimensional symbols for a NC unit are shown in Fig. 1b. *W* is the waist width of a single NC pattern and the gap between the tips of two opposite NC for the paired case is denoted as '*G*'.

Schematic of the fabrication process for NC patterns is provided in Fig. 1c. First, photoresist (ZEP-520A, Zeon Co. Ltd., Japan) was uniformly spin-coated onto a clean quartz wafer (Plan Optik, Germany), followed by EBL to accurately define the shapes of NC. After developing, 5 nm Ti (titanium) and 30 nm Au thin films were sequentially deposited onto the photoresist-patterned substrate. The bottom metal layer (Ti) here was adopted to enhance the adhesion between the top Au layer and the substrate. Finally, lift-off process was introduced to remove the photoresist residual together with the metals on top. Such fabrication process is also suitable for single NC patterns which are not described in the figure.

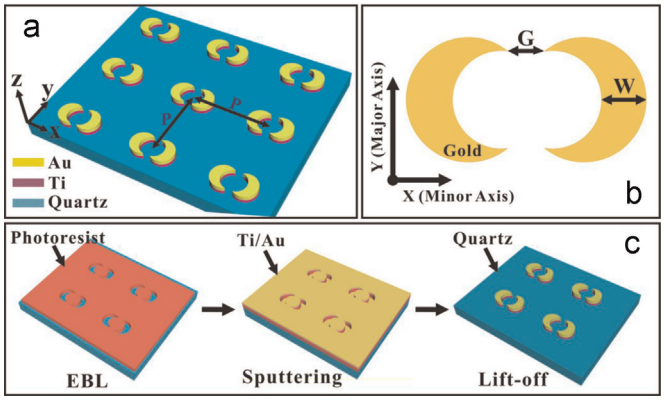

Fig. 1. (a) 3D configuration of NC arrays on a quartz substrate; (b) dimensional parameters of an individual NC unit; (c) fabrication process of paired NC arrays on a quartz substrate. The schematic is also suitable for fabrication of single NC patterns (not depicted in the figure).

2.2. Characterization of NC arrays

In this work, three different NC samples were fabricated on quartz substrate with well-defined morphologies and the covering area of the pattern array for each design is around 2 cm^2. For all NC arrays, the periodicity is set to be 600 nm in both of the major and minor axes. The top picture of Fig. 2a shows the atomic force microscope (AFM) image of sample S1 (single NC) and the enlarged scanning electron microscope (SEM) image that shows a waist width of around 111 nm. The AFM image also confirms the actual height of the NC that is corresponding to the processing parameters. SEM images of sample P2 and P3 (paired NC) are given which shows the different dimensional values of the two samples. For P2, *W* is around 86.3 nm and *G* is around 62.5 nm. For P3, *W* is slightly decreased to around 66.7 nm and *G* of around 43.3 nm. We can clearly observe from the SEM images that the gap between two opposite NC tips in P3 is smaller than that in P2. Such structural difference can be accurately regulated via the well-developed EBL fabrication technique. The LSPR properties of such obtained NC patterns were further characterized via UV/vis spectrometer Lambda 20 (Perkin Elmer, Massachusetts, USA) within wavelength range of 550–1100 nm based on the transmission geometry. Fig. 2b (top) shows the experimental normalized transmission spectra upon normal incidence of the excitation source with electric field polarization parallel to the minor axis. The spectral peak positions of samples S1, P2 and P3 were experimentally observed to be 852 nm, 866 nm and 938 nm, respectively.

The theoretical transmission spectra and electric field distributions were calculated via COMSOL 4.3b commercial package. Detailed simulation parameters were described in the Supporting information. Simulated transmission spectra of the three samples were provided in the bottom of Fig. 2b. The calculated dip position under such resonant modes was found to be of 844 nm, 872 nm, and 938 nm. It could be noticed that the experimental resonant peaks were slightly deflected from the simulated results. Such mismatch may be induced by the structural difference between the real sample and the theoretical models. Furthermore, the relative broad FWHM (full width at half maximum) of the experimental spectra may be caused by the dimensional deviation of the nano-patterns raised during the fabrication process. From this perspective, good agreement can generally be concluded between the measured spectra and the simulation results.

The electric field distributions of off-resonant and on-resonant excitation wavelengths were also figured out for all three samples (Fig. 2c). The color legends show the values of the enhancement factor of the electric field, E/E_0, where E_0 is the electric field component of the illumination as described in the Supplementary information. Take S1 as an example, the strength of the electric field near the NC tips can be found to be dramatically enhanced at the wavelength (840 nm) around the resonant peak when compared to the off-resonance wavelength (560 nm). In addition, the field distributions can clearly exhibit the enhancement is mainly localized near the tips and attributed to the dipole resonance mode with electric field polarization perpendicular to the major axis (Cooper et al., 2014). Such phenomenon can also be obviously confirmed from the field distributions of the paired NC samples (P2 and P3).

2.3. Microfluidic chip-controllable concentration gradient generator

To dynamically generate concentrations for real-time detection in the microfluidic system, a concentration gradient generator was